Mechanistic insights and clinical implications of cross-reactive anti-prophage antibodies and bacterial heteroresistance on phage therapeutic failure

Gordillo Altamirano F[1,2,#], Subedi D[2,3], Beiers M[1], Bucher M[3], Dahlman S[3], Patel DM[4], Parker M[1], Korneev D[5], Pragastis K[1], Wisniewski J[1], Rees C[6], Ramshaw H[4], Khan SF[1,7], Gardiner BJ[1], Hammerschlag Y[1], Keating D[8], Kotsimbos T[8], Hawkey J[1], Barr JJ[2,3], Peleg AY[1,2,9*]

[1]Department of Infectious Diseases, Alfred Health and School of Translational Medicine, Monash University, VIC, Australia
[2]Centre to Impact AMR, Monash University, VIC, Australia
[3]School of Biological Sciences, Monash University, VIC, Australia
[4]Antibody Discovery Platform, Monash University, VIC, Australia
[5]Ramaciotti Centre for Cryo-Electron Microscopy, Monash University, VIC, Australia
[6]Melbourne Water Corporation, VIC, Australia
[7]Microbiology Unit, Department of Pathology, The Alfred Hospital, Melbourne, VIC, Australia
[8]Department of Respiratory Medicine, The Alfred Hospital and School of Translational Medicine, Melbourne, VIC, Australia
[9]Infection Program, Monash Biomedicine Discovery Institute, Department of Microbiology, Monash University, VIC, Australia

#Lead author: Dr Fernando Gordillo Altamirano MD MMed PhD
fernando.gordilloaltamirano1@monash.edu

*Corresponding author: Professor Anton Y. Peleg MBBS PhD MPH FRACP FAHMS
anton.peleg@monash.au

Abstract

Phage therapy is an exciting strategy against antimicrobial-resistant bacterial infections, but critical knowledge gaps regarding its clinical application persist. Studying a patient with a life-threatening, chronic bacterial infection who failed phage therapy, we uncovered important biological concepts with direct translational impact. Using longitudinal clinical samples, we found that patients can harbour pre-existing antibodies against active prophages induced from the genome of the causative pathogen. Notably, these antibodies can contribute to clinical failure by cross-reacting with and effectively neutralising therapeutic phage. We also uncovered bacterial heteroresistance, characterised by bacterial subpopulations from the initial infection with reduced phage susceptibility, as a further contributor to treatment failure. These findings highlight the intricate interplay between host immunology, bacterial genetic diversity and phage biology, bearing broad significance for clinical phage therapy. Future phage therapy patients, especially those with chronic infections, should be screened for antiphage immunity and bacterial heteroresistance prior to phage treatment.

Introduction

Antimicrobial resistance (AMR) is one of the greatest health threats we currently face. The latest global estimations suggest that in 2021, bacterial AMR directly caused over a million deaths, while playing a role in just under 5 million [1]. AMR is not only a leading cause of death but poses a significant burden on the global economy and healthcare systems [2]. These consequences are expected to increase unless a concerted, multi-disciplinary effort is deployed to fight AMR, including the development of therapeutic strategies for when antibiotics prove ineffective, such as phage therapy.

Phage therapy is the clinical use of bacteriophages, viruses that specifically kill bacteria, to treat bacterial infections [3]. Although phages were discovered and used before antibiotics, phage therapy is now experiencing a resurgence amidst the AMR crisis. In the last two decades, we have accumulated a significant body of evidence from preclinical studies suggesting that phage therapy is safe and potentially effective [4], encouraging translational efforts. As for clinical use, a recent systematic review examined 2,241 patients from 59 studies and deemed phage therapy a promising strategy in the fight against difficult-to-treat infections and AMR [5]. However, most of this clinical experience comes from case reports and case-series, with only a handful of clinical trials. Substantial knowledge gaps remain to be addressed before phage therapy becomes standardised and widespread, including questions around the pharmacology of phages, their interactions with antibiotics, and the tripartite relationship between phages, bacteria and the human host [6].

We present a patient with a chronic, extensively drug-resistant (XDR) bacterial (*Bordetella bronchialis*) infection associated with life-threatening infective pulmonary exacerbations and bacteraemia that was poorly controlled with traditional antibiotics. The patient qualified for compassionate use phage therapy. We report the isolation and detailed characterisation of the therapeutic phage, and the clinical course of the patient that resulted in phage therapeutic failure with bacteriological relapse. We explored the complex *in vivo* dynamics of host immunology, bacteriology, and phage biology, and have provided essential clinical insights into the future treatment of life-threatening bacterial infections with bacteriophages.

Results and Discussion

Recurrent life-threatening infection with extensively drug-resistant bacteria

A 22-year-old male patient with cystic fibrosis (CF) was referred to the Victorian Bacteriophage Therapy Program (VIC*Phage*) in 2022 for compassionate use phage treatment of recurrent, invasive *Bordetella bronchialis* infection, including pneumonia and bacteraemia. He had a history of a liver-pancreas transplant six years prior for CF-related liver disease and diabetes mellitus, and end-stage kidney disease secondary to calcineurin inhibitor use, aminoglycoside exposure, and diabetes mellitus. He was on maintenance immunosuppression with tacrolimus and prednisone.

B. bronchialis was first isolated from the patient's sputum at the age of 10 years. *B. bronchialis*, known before 2015 as *Bordetella* genogroup 3, are clinically uncommon motile Gram-negative bacilli that are

82 facultatively aerobic and slow-growing [7]. Despite reported cases of this pathogen in patients with CF
83 [8,9], there is limited information regarding its pathogenesis, biology, or epidemiology. Through his
84 teenage years, the patient developed recurrent infective respiratory exacerbations with repeated
85 hospitalisation and isolation of *B. bronchialis*. Initially, the isolate tested susceptible to ceftazidime and
86 piperacillin-tazobactam (Table S1). However, repeated infections ensued and in the three years prior to
87 referral, he was admitted nine times for infective exacerbations, including three episodes of invasive
88 bacteraemia, an uncommon complication in patients with CF. To prevent or reduce the frequency of
89 these life-threatening exacerbations, ongoing minocycline and trimethoprim-sulfamethoxazole were
90 commenced in 2021.
91
92 In June 2022, the patient presented with fever, productive cough, and dyspnoea. Breakthrough *B.*
93 *bronchialis* was isolated from sputum and multiple sets of blood cultures. Chest imaging demonstrated
94 diffuse, severe bilateral bronchiectasis with extensive mucous plugging and patchy foci of consolidation.
95 He was commenced on empiric IV meropenem and inhaled colistin, and antimicrobial susceptibility
96 testing demonstrated that the isolate had become XDR (Table S1, Note S1). At this point, referral for
97 compassionate use phage treatment was received.
98
99 **Isolation and characterisation of an active phage**
100 Using wastewater samples from Melbourne, Australia, and cultures of a single *B. bronchialis* colony
101 obtained from the patient's sputum in June 2022 (wild type [wt] *B. bronchialis*), we successfully
102 discovered, isolated and amplified phage øSimón (Fig. 1a). Multiple efforts to isolate additional phages
103 were unsuccessful. In liquid coculture, øSimón inhibited bacterial growth for up to 40 hours at
104 multiplicities of infection (MOI) as low as 0.01 (Fig. 1b), and consistently achieved titres above 10^8
105 plaque forming units (pfu)/ml. In a one-step kill curve, we determined that øSimón had a latency time
106 of 150 min and a burst size of nearly 30 virions per cell (Fig. 1c). øSimón displayed similar activity
107 against five other clinical *B. bronchialis* isolates (three from blood, two from sputum) obtained from the
108 patient prior to starting phage therapy (Fig. 1d). Transmission electron microscopy (TEM) showed that
109 øSimón was morphologically a siphovirus, with a total length of ~226 nm (Fig. 1e). øSimón's genome
110 did not encode for any markers of lysogeny, AMR, toxins or virulence (Fig. 1f, Note S2), making it an
111 ideal candidate for therapeutic use.

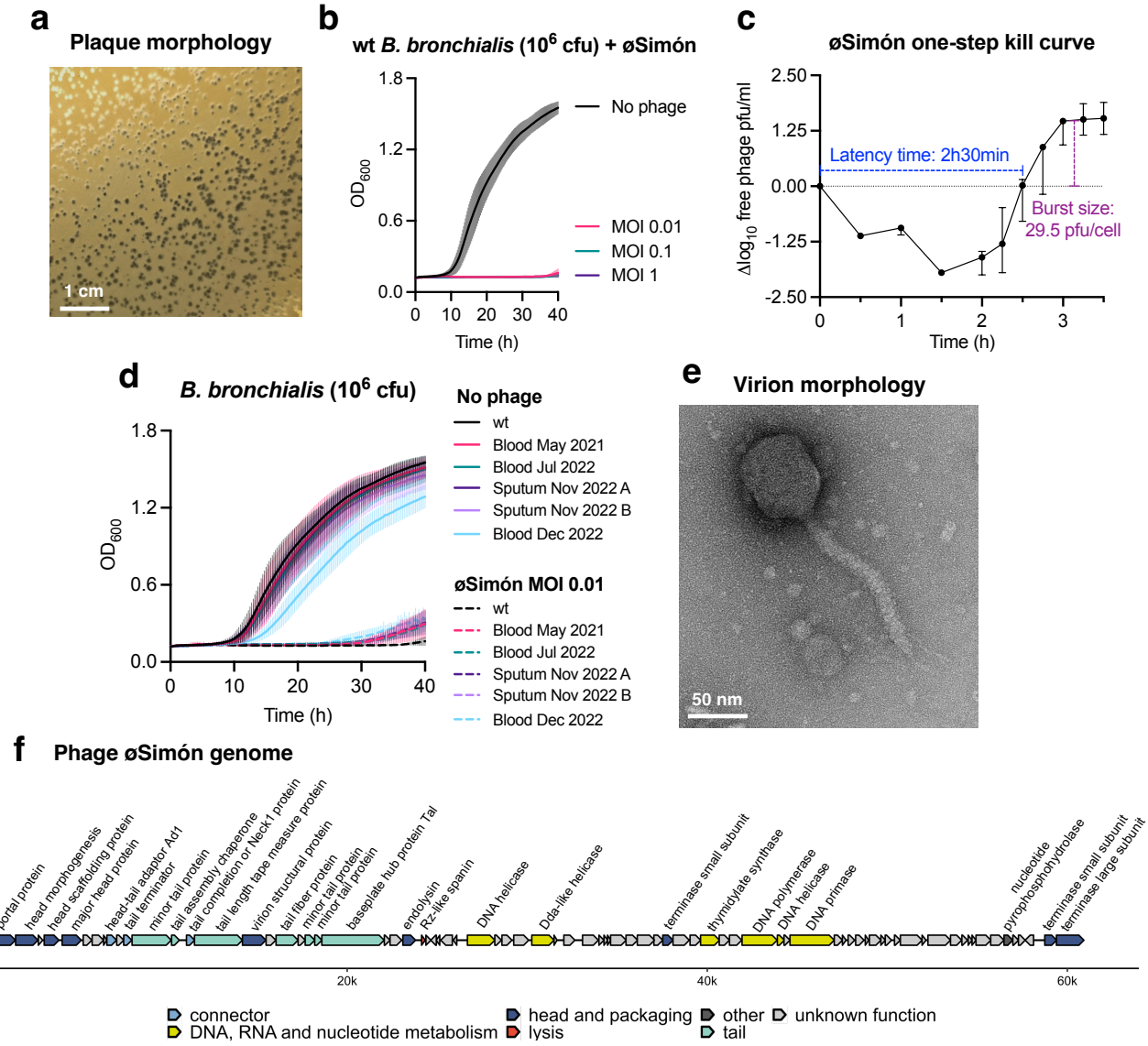

Figure 1. Characterisation of phage øSimón. a: Plaque morphology on HI agar, 48 h of incubation. Scale bar: 1 cm. **b:** Optical density at 600 nm (OD_{600}) growth curve (mean ± SD; n = 3) of *B. bronchialis* without phage (black) and with three different multiplicities of infection (MOI) of øSimón. **c:** One-step kill curve (median ± 95% CI; n = 3). **d:** Sensitivity of further *B. bronchialis* isolates from the patient against øSimón in liquid culture (growth curve, mean ± SD; n = 3). Isolates are labelled by type of clinical sample and date of isolation. **e:** øSimón virion under transmission electron microscopy. Scale bar: 50 nm. **f:** Assembled øSimón genome (60,921 bp, 80 open reading frames).

Clinical administration of øSimón

A clinical-grade preparation of øSimón was produced locally at the Monash Phage Foundry. All product batches (Table S2) underwent internal and third-party validation for sterility and endotoxin levels suitable for IV administration [10]. In the setting of a repeated episode of invasive bacteraemia with XDR *B. bronchialis*, the patient received the first dose of IV øSimón (5.4×10^7 pfu/dose) (day 0) (Fig. 2). Phage therapy was administered twice daily and, given the severity of infection, was co-administered alongside

IV meropenem and inhaled colistin. The patient stabilised clinically, with blood cultures clearing by day 5. After close clinical and laboratory monitoring for six days, the patient was transferred to our hospital-in-the-home program for ongoing IV phage management, completing 30 days [11]. Phage therapy was well tolerated, with no clinical or laboratory adverse effects reported.

Alongside these clinical outcomes, we observed an almost 80% reduction in the amount of *B. bronchialis* in the patient's sputum at day 8 of phage treatment, and notably, this coincided with the finding of actively replicating øSimón (Fig. 2). However, by day 17, the *B. bronchialis* load increased back to pre-treatment levels, and øSimón was no longer isolated from the sputum. The patient went on to develop progressive complications of his end-stage renal disease. In the context of a repeat admission for worsening illness (day 68), he developed further episodes of *B. bronchialis* bacteraemia and passed away on day 93, two months after the last dose of øSimón. Given the undulating clinical and microbiological course, we investigated the possible mechanisms of phage therapy failure and the dynamic interactions between bacteria, phage and human host over time.

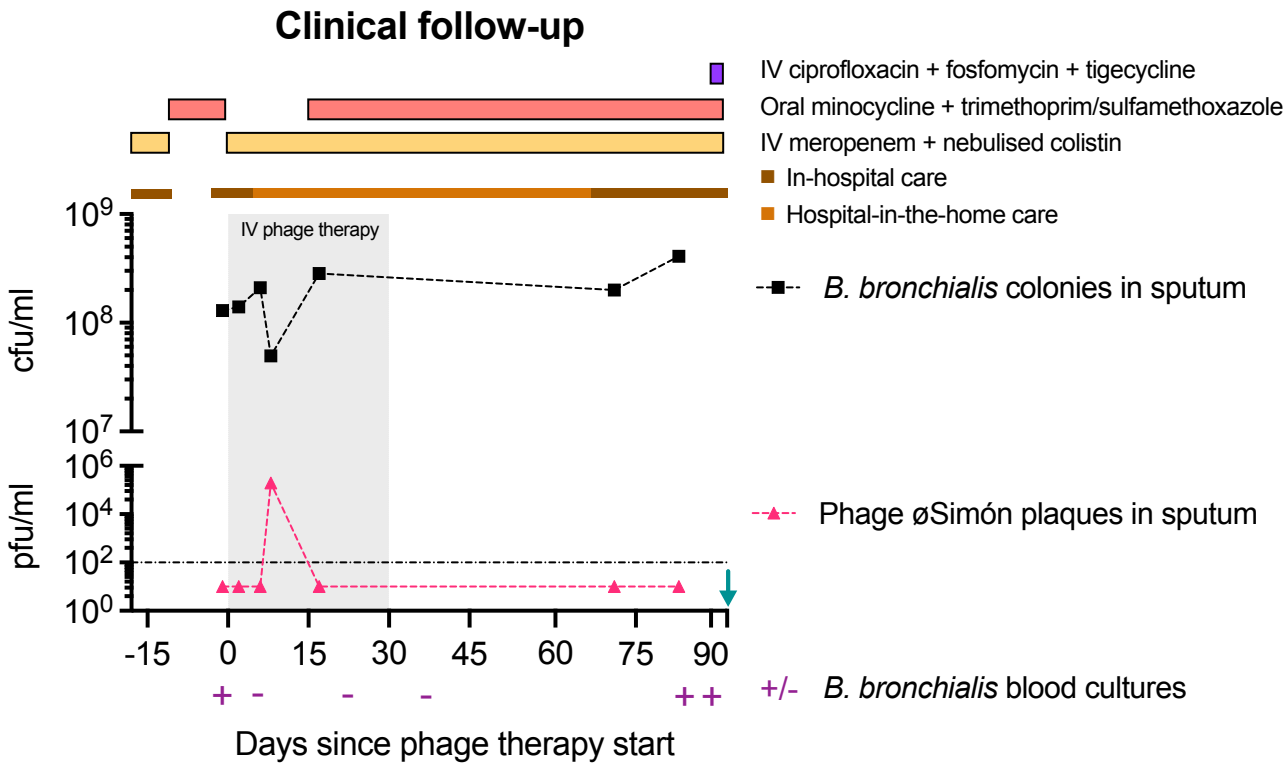

Figure 2. Clinical follow-up of phage therapy. The patient received the first dose of phage therapy on Day 0 (Dec 20th, 2022) and passed away on day 93 (teal arrow). The grey shade in the plot represents the 30-day period of IV phage therapy. Laboratory tests included blood cultures for *B. bronchialis* (positive [+] and negative [-] symbols under the x-axis), and quantification of *B. bronchialis* and øSimón in the patient's sputum (n = 1, three technical replicates each). Dotted line at y = 10^2 highlights the limit of detection of the sputum assays. Atop the graph, coloured rectangles denote antibiotic therapy administered to the patient, and the coloured line differentiates between inpatient and outpatient care.

Pre-existing antiphage immunity

Despite phages being non-pathogenic to humans, it has been confirmed that the human immune system produces antibodies against them [12]. Antiphage antibodies can neutralise phage activity [13], but how much this immune response, or lack thereof, contributes to the outcomes of phage therapy is still debated [14-17]. This humoral response is T-cell dependent, and activated B-cells produce a specific, polyclonal, antiphage antibody response [12,18]. Circulating antibodies usually peak one to two weeks after initial contact with a phage [12,19], aligning with the time we observed a reduction of phage activity in our patient.

Using patient serum samples from days 0, 7, and 21, we first performed a phage neutralisation assay [17]. Briefly, we tested the ability of three successive 10-fold serum dilutions to neutralise a known dose of øSimón in 30 min. We used an unrelated, anti-*Pseudomonas aeruginosa* phage (øFaith) as a control under the same conditions. Notably, at day 0, before the patient had received the first dose of øSimón, the serum could neutralise ~25% of the phage dose (Fig. 3a). The neutralisation increased to ~60% on days 7 and 21. No neutralisation was seen against the control phage. We also used a more standardised metric known as the phage inactivation rate (*k*), which generates “high”, “moderate”, and “low” thresholds, inversely correlating with odds of treatment success [15,17]. We showed that the patient’s pre-treatment serum had a “moderate” *k* value of 10.69, which increased to “high” at days 7 and 21 (27.67 and 30.60, respectively) (Fig. 3b). Interestingly, we also observed low phage neutralisation capacity in the patient’s sputum (Fig. 3c and 3d).

To confirm that the phage inactivation was mediated by anti-øSimón antibodies, we designed an indirect ELISA assay. Intact clinical-grade øSimón was used as the coating antigen. To further discriminate the presence of confounding antibodies against endotoxin or other bacterial products, we also used a vehicle control obtained by filtering out (0.02 μm) phage particles from the coating product. Sera from the patient were run in parallel with a serum control from a healthy patient, and all tests used an isotype pan-specific detection antibody. The ELISA confirmed the presence of anti-øSimón antibodies at days 0, 7, and 21, with no quantitative differences between days (Fig. 3e). Anti-øSimón antibodies were also detected in the patient’s sputum, although the signal was markedly less intense than in serum (Fig. 3f). Interestingly, a significant peak of antibody was detected in the sputum on days 8 and 17, while the patient was receiving IV phage therapy, compared to follow-up sputum from day 84, almost two months after phage therapy had stopped. To summarise, we demonstrated the presence of antibodies capable of recognising and inactivating øSimón in both serum and sputum of the patient even prior to phage therapy. These antibody levels were maintained throughout the duration of therapy and beyond, but their neutralising effect increased over time, suggesting affinity maturation [20].

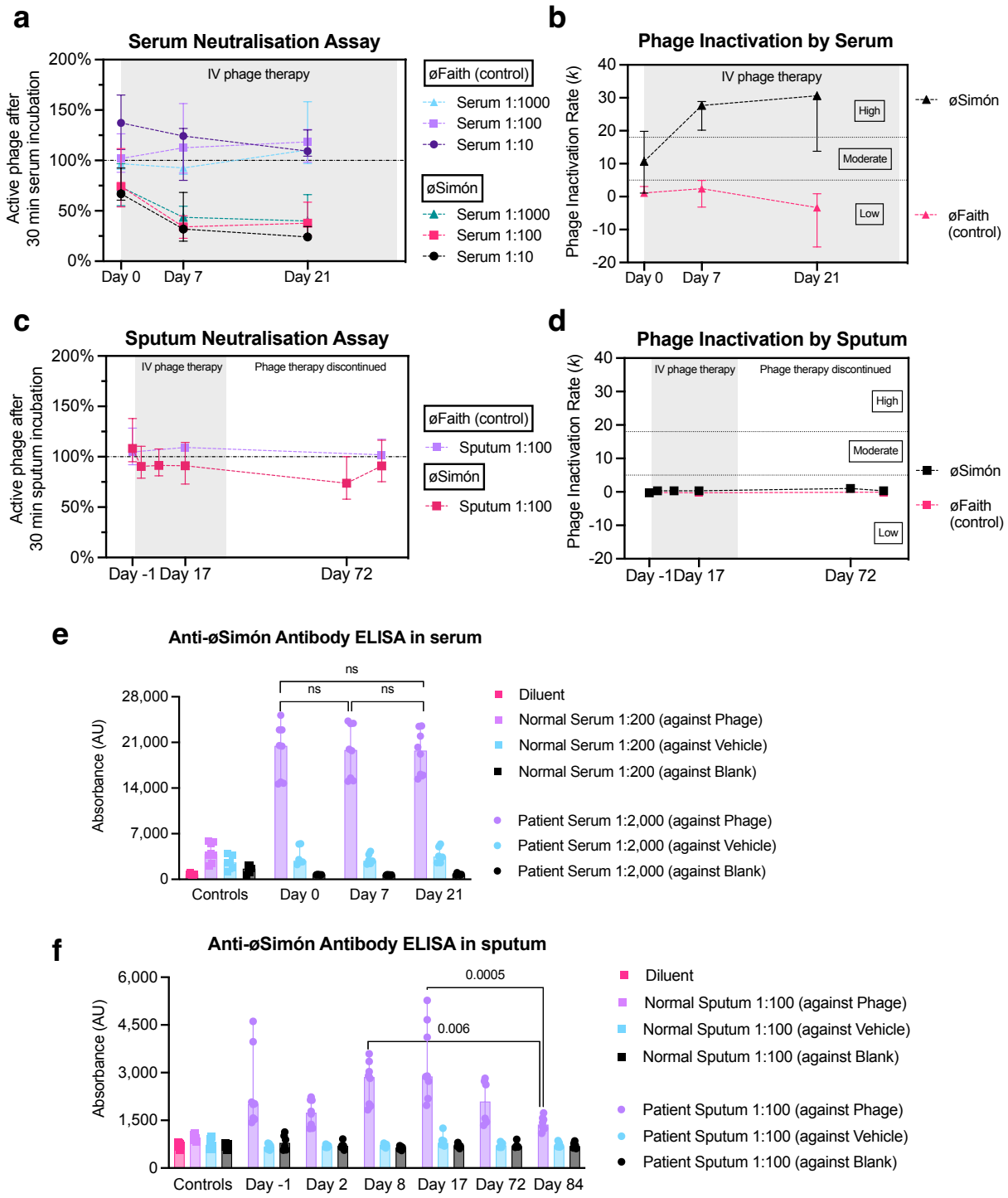

Figure 3. The patient harboured pre-existing antiphage immunity. a: Serum neutralisation assay (10^6 pfu). The x-axis follows the treatment timeline, and the y-axis plots the percentage of active phage (soft overlay agar assay) (median ± 95% CI; n = 3). **b:** Calculation of phage inactivation rate (*k*) with data from the previous assay (median ± 95% CI; n = 3). **c and d:** The experiments depicted in a and b were repeated using patient's filter-sterilised sputum instead of serum. **e and f:** Indirect ELISA looking for anti-øSimón antibodies in serum (e) and sputum (f). Controls were run with serum from a healthy donor or sputum from a patient with cystic fibrosis (median ± 95% CI; all replicates plotted; n ≥ 6; Kruskal-Wallis test; if not plotted the comparison was not statistically significant).

196 **Resident prophages driving pre-existing immunity to therapeutic phage**
197 We investigated a possible explanation for the presence of pre-existing anti-øSimón antibodies. Given
198 the seemingly infinite diversity of phages in the biosphere [21], we believe it was unlikely for the patient
199 to have previously encountered øSimón. However, as the patient had harboured the *B. bronchialis*
200 infection for over a decade, we hypothesised he may have been exposed to other phages with activity
201 against the pathogen, sharing similar structural features to øSimón, and triggering a cross-reactive
202 immune response. Furthermore, recent studies using cell-free DNA sequencing have demonstrated that
203 patients with sepsis have an overrepresentation of pathogen-specific phages [22,23]. This could be
204 explained by prophages, which are phages that have integrated into a bacterium's chromosome and
205 occasionally re-enter the lytic cycle in periods of rapid bacterial expansion or stress [23]. Consequently,
206 we sought to investigate whether prophages integrated into the patient's *B. bronchialis,* and reactivated
207 at different times during the chronic infection, could have been responsible for cross-reactive immunity
208 against øSimón.
209
210 We parsed the genome of the wt *B. bronchialis* for prophage regions. We identified three prophages
211 with medium-to-high completeness scores [24]. On a nucleotide level, they did not show homology to
212 øSimón (Fig. 4a, S1a). Next, we explored whether these prophages could re-enter the lytic lifecycle by
213 the addition of an induction agent, the antibiotic mitomycin C, to a bacterial liquid culture, or
214 spontaneously in the absence of an induction agent. After purification, we confirmed the presence of
215 phage virions through TEM and DNA sequencing, but only in the culture with mitomycin C. TEM
216 micrographs of the suspension detected phage particles at a concentration of ~10^6 virions/ml, with a
217 single (siphovirus) morphology (Fig. 4b). After sequencing, two thirds of the obtained reads mapped to
218 prophage region 2, a 51.5 kb-long sequence with the closest match being *Burkholderia* phage Bups
219 phi1 (GenBank accession numbers EU307292.1-EU307295.1), also a siphovirus. This lysate,
220 containing at least one of the induced prophages from the *B. bronchialis* host, was then used for
221 subsequent experiments.
222
223 Using the induced prophage suspension, an ELISA was developed to detect anti-prophage antibodies,
224 which were confirmed in the patient's serum but not sputum (Fig. 4c and S2). Although the antibody
225 signal was weaker than in the assays for anti-øSimón antibodies, the two assays are not directly
226 comparable. The concentration of virions in the solution used to coat the ELISA wells was 100-times
227 lower for the induced prophage. We then tested for cross-reactivity between the anti-prophage and anti-
228 øSimón antibodies. To do this, we modified our indirect ELISA protocol to include a pre-capture step,
229 where the serum was passaged on wells coated in one of three conditions in parallel: 1) blank or PBS,
230 2) øSimón virions, or 3) induced prophage virions. After this, the ELISA was run as usual, checking for
231 anti-prophage antibodies (Fig. 4d). Theoretically, the first condition would give the maximum signal, and
232 the third condition would give the lowest, with the signal in the second condition being representative
233 of the presence or absence of antibodies capable of recognising both øSimón and the prophage. As
234 shown in Fig. 4e, we observed an equal reduction in the signal of anti-prophage antibodies when using
235 øSimón or prophage pre-capture (median = 17% vs. 24%, $p = 0.09$), indicating that most anti-prophage

antibodies were capable of recognising øSimón. When the assay was instead used to measure the anti-øSimón antibody signal under the three conditions, we observed that pre-capture with øSimón reduced the signal of anti-øSimón antibodies (median = 18%), but pre-capture with prophage resulted in a negligible signal reduction (median of 0.8%, p = 0.766 against pre-capture with PBS). This suggested that the anti-prophage antibodies were not the only antibodies in the patient's serum capable of recognising øSimón.

Together, our data provided experimental confirmation that the human body can produce antibodies that recognise induced prophages from a resident bacterial pathogen. These same antibodies were capable of cross-reacting with the therapeutic øSimón. This prophage-to-øSimón antibody cross-reactivity provides a partial explanation for the neutralisation activity of the patient's pre-treatment serum and the potential impact on øSimón efficacy. Our results complement two important earlier findings. First, Halperin *et al*. showed that patients with acute glomerulonephritis produced antibodies against a secreted, prophage-encoded, streptococcal hyaluronidase [25]. Second, Fluckiger *et al*. demonstrated T-cell-mediated immunity aimed at a specific tail length tape measure protein from an enterococcal prophage in mice and humans, which cross-reacted with tumour-associated antigens [26]. Taken together, there is a growing body of evidence showing the relevance of prophages and their interactions with the immune system in various states of human health and disease.

Future endeavours in this area could include establishing the precise proteins or epitopes responsible for the observed cross-reactivity. We note, for instance, that at the amino acid level, prophage region 2 has a gene coding for a minor tail protein, with a modest homology to øSimón (29% amino acid identity, 87% query coverage) (Fig. S1). Berkson *et al*. have demonstrated that cross-reactive humoral immunity between two therapeutic myoviruses in a phage cocktail was possibly mediated by tail fibre, tail sheath, and major capsid proteins as antigens [27]. Other areas worth exploring are the precise impacts of antibody titre and affinity on phage pharmacokinetics at different body sites and quantifying their consequence on therapeutic effects.

a

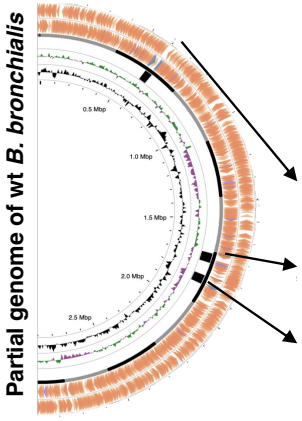

Prophages in the wt *B. bronchialis* genome

Prophage Region	Length	Completeness Score	Most Similar Genome (MSG)	MSG Morphology	% Mapped reads after Induction
1	39.9 kb	77 (Medium)	Bordetella phage vB_BbrS_PHB09	Siphovirus	0%
2	51.5 kb	86 (Medium)	Burkholderia phage Bups phi1	Siphovirus	67%
3	48.5 kb	91 (High)	Ralstonia phage RSY1	Myovirus	33%

b

Induced prophage virion morphology

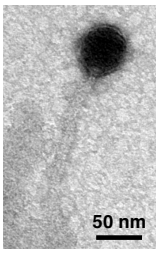

c

Anti-Prophage Antibody ELISA in serum

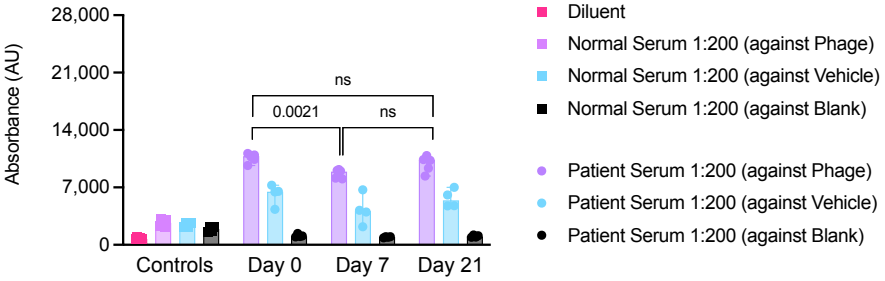

d

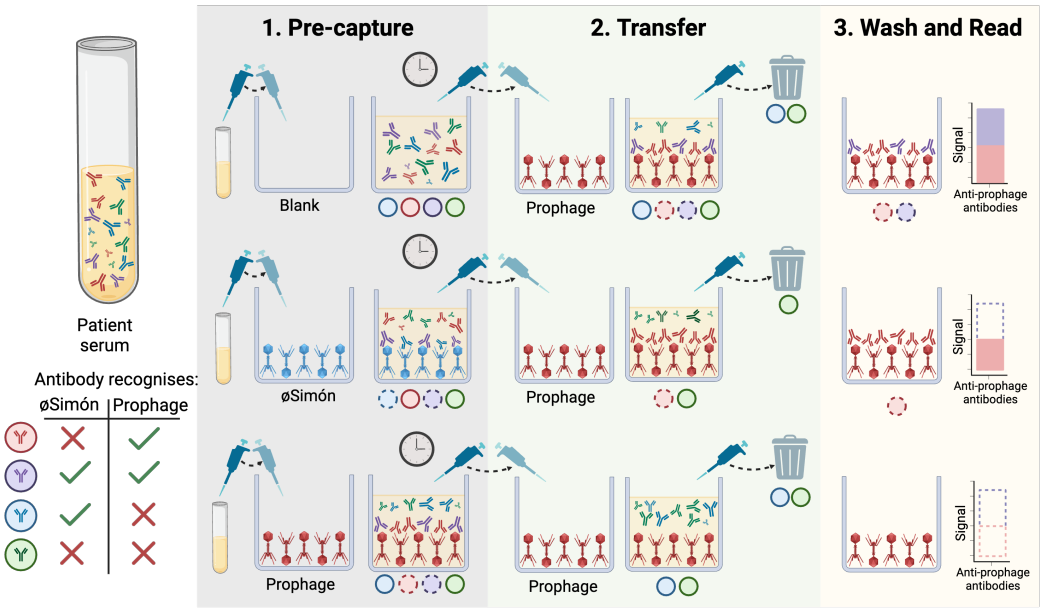

e

Pre-capture ELISA (1:2,000 Day 0 serum in PBS)

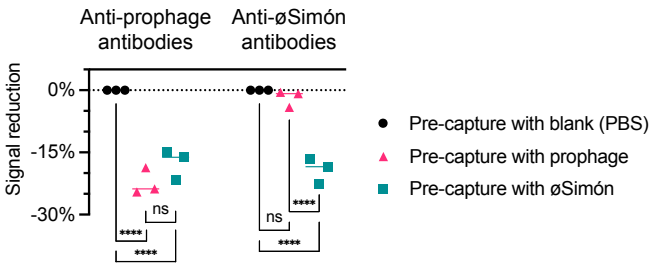

263

Figure 4. *Bordetella bronchialis* prophages were partly responsible for the pre-existing immunity. a: Screening of prophage regions in the genome of wt *B. bronchialis.* Rings from innermost to outermost: genome length, GC%, GC skew and open reading frames. The adjacent chart provides information about the three prophages found. **b:** Transmission electron micrograph of the virions found after a culture of *B. bronchialis* was treated with mitomycin C for prophage induction. Scale bar = 50 nm. **c:** Indirect ELISA looking for anti-prophage antibodies in serum; (median ± 95% CI; all replicates plotted; n ≥ 4; Kruskal-Wallis test; ns: not significant). **d:** Experimental setup for the pre-capture ELISA. Hypothetical antibodies colour-coded by their ability to recognise øSimón (blue), prophage (red), both (purple), or neither (green). Pre-capture step (1), serum is passed through wells that have been coated with either PBS (blank, top), øSimón (blue virions, middle), or prophage (red virions, bottom). The circles beneath wells represent the colour-coded antibodies either binding to phages (dashed border) or remaining in suspension (solid border). Next, the serum is transferred to fresh, prophage-coated wells (2), left for incubation and binding, and discarded. All unbound antibodies are washed away, and the signal is read (3). The assay is interpreted by measuring the signal reduction between the top condition and each of the remaining two. Not shown in the figure, the assay was later repeated using øSimón to coat wells in step (2). **e:** Pre-capture ELISA. Percentage reduction was calculated using the reading for the PBS pre-capture condition as baseline (bars are medians, all replicates plotted; 2-way ANOVA for comparisons; ns: not significant, **** $p < 0.0001$).

Bacterial heteroresistance as a risk for treatment failure

Bacteria can use a vast repertoire of mechanisms to resist phage infection [28,29], and previous reports have demonstrated emergence of phage resistance during phage therapy [30-33]. While this phenomenon can sometimes be beneficial, for example leading to collateral loss of antibiotic-resistance resulting in phage-antibiotic synergy [31,33,34], it can also be the cause for treatment adjustment [35], or failure [32]. Therefore, we investigated if resistance to øSimón emerged during treatment, possibly contributing to the observed therapeutic failure.

We first assessed the ability and mechanism of the patient's *B. bronchialis* to develop resistance to øSimón *in vitro*. After spotting øSimón on a lawn of wt *B. bronchialis*, we observed colonies growing in the middle of a lysis zone. We purified one of these colonies, confirmed it was phenotypically resistant to øSimón and sequenced its genome. Pairwise genomic comparison found that this isolate harboured a single mutation, a one-nucleotide insertion leading to a frameshift and premature stop codon in the gene *btuB,* coding for the outer membrane vitamin B12 receptor of the same name (Fig. 5a). The BtuB-deficient strain grew in the presence and absence of øSimón (Fig. 5b), and an adsorption assay revealed that øSimón virions did not adsorb to this bacterial host (Fig. 5c). BtuB has been previously confirmed as either a sole, dual, or co-receptor for phages infecting the genera *Salmonella, Yersinia* and *Escherichia* [36-39]. All of this suggests that øSimón needs BtuB for adsorption and that, as seen for many other phage-host pairs [40], loss of receptor function is a mechanism of *B. bronchialis* resistance to øSimón *in vitro*.

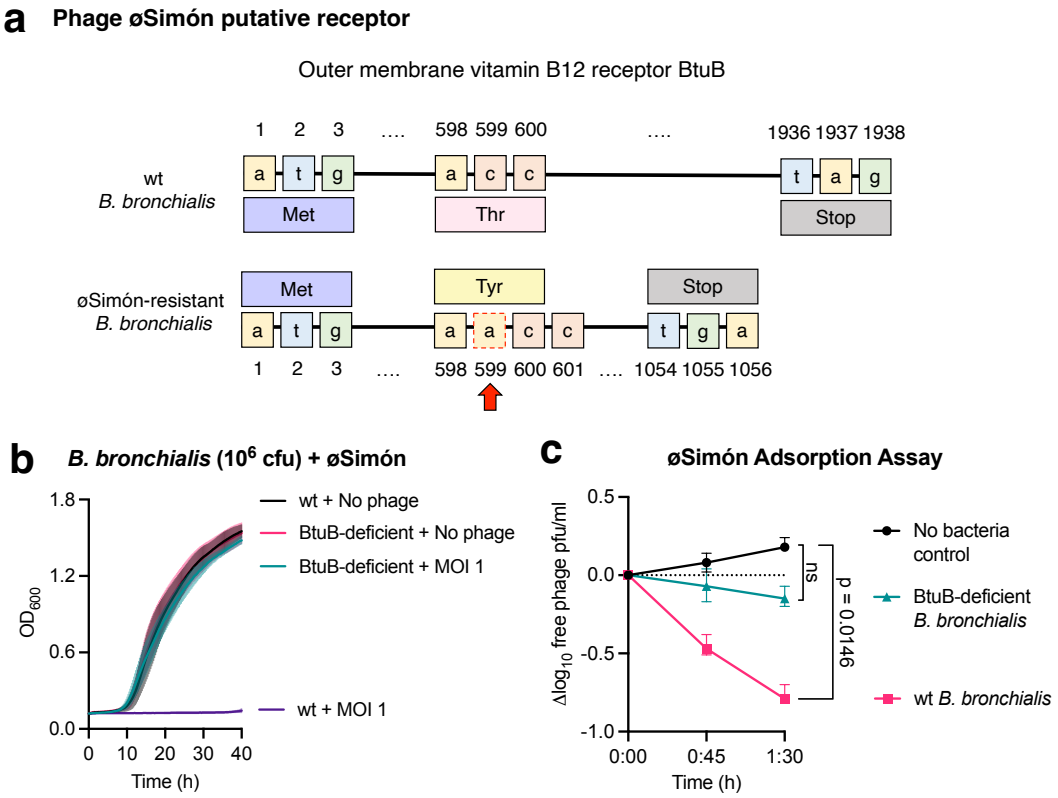

Figure 5. *In vitro* mechanism of resistance against phage øSimón. a: Representation of the *btuB* gene sequence in wt *B. bronchialis* (top) and a mutant resistant to øSimón (bottom). The red arrow and box indicate the insertion of an alanine at position 599, leading to a premature stop codon in the phage-resistant bacterium. **b:** Bacterial growth curves of wt *B. bronchialis* and the BtuB-deficient variant presented in panel (a), with and without phage (mean ± SD; n = 3). **c:** Adsorption assay of øSimón to wt or BtuB-deficient *B. bronchialis* over 90 minutes (median ± 95% CI; n = 3; Kruskal-Wallis test).

We then analysed the patient's sputum samples over time for the presence of phage-resistant bacteria. Instead of starting our screening with individual colonies grown from each sputum sample, we took a population-wide approach. We adapted the inverted spot assay technique [41] whereby a high concentration of øSimón was used as a selection marker on semisolid media to detect putative phage-resistant *B. bronchialis*, with species confirmation performed using MALDI-ToF MS (Fig. 6a). This method allowed us to compare the number of *B. bronchialis* colonies that grew in the absence of øSimón (general population) against the number that grew in its presence (putative resistant population), thus calculating a ratio (Fig. 6b). Surprisingly, we discovered that before phage administration (day -1), a median of 2.3% (range: 1.7% to 11.6%) of the *B. bronchialis* population appeared to resist øSimón. This finding suggested baseline heteroresistance, defined as the presence of bacterial subpopulations with varied susceptibility to an antimicrobial (øSimón in this case), a phenomenon capable of contributing to treatment failure [42]. To further investigate for heteroresistance, we randomly chose and purified 14 bacterial colonies from the pre-treatment sputum sample (day -1) and tested their efficiency of plating (EOP) for øSimón. A range of EOPs were identified across these pre-treatment colonies with most of

them having values below 1, indicating reduced susceptibility to øSimón (Fig. 6c). These data supported the findings that the patient was infected with a heteroresistant population of *B. bronchialis.*

During and after treatment, the proportion of sputum colonies able to grow in the presence of phage remained relatively stable, but it reached a peak of 5.3% at day 17, coinciding with the bacteriological relapse seen in the patient (Fig. 2 and 6b). We randomly picked 6 to 8 colonies from the phage-selection plates (Fig. 6a) at each timepoint after initiating phage therapy (days 2, 6, 8, 17, 72 and 84, n = 44 colonies) and performed spotting and EOP assays with øSimón. In this subset, we also observed a range of EOPs, including five strains that were completely resistant to øSimón (EOP below the limit of detection of 10^{-7}) (Fig. 6d). Mirroring the range in EOPs, we also observed variations in the size and/or clarity of the plaques øSimón produced on the isolates (Fig. 6d). Together, these findings revealed that before, during and after phage therapy, the patient harboured a bacterial population that was not uniformly sensitive to øSimón, and that instead of a sensitive/resistant dichotomy, the effectiveness of øSimón against the patient's *B. bronchialis* fell within a spectrum. This solidified the hypothesis of heteroresistance and prompted an exploration of its genetic basis.

Genetic analysis of bacterial heteroresistance

Using short-read whole genome sequencing of all 58 isolates (14 pre-treatment and 44 post-treatment) compared to the assembled genome of the wt *B. bronchialis* (host of isolation of øSimón, June 2022), we identified broad diversity, with two major clusters and several subclusters (Fig. 6e). Cluster 1 housed the wt strain, 3 of the 14 (18%) pre-treatment isolates, and 9 of the 44 (20%) post-treatment isolates. Cluster 2 was larger and included the remaining 11 pre-treatment and 35 post-treatment isolates. Using a SNP distance matrix (Fig. 6f) we noticed that the cluster differentiation corresponded to the EOP of the pre-treatment strains. Namely, all 3 strains belonging to cluster 1 had an EOP > 1 indicating high susceptibility to øSimón, whereas 9 of the 11 strains from cluster 2 had an EOP < 1. We then screened for specific genes and mutations that may explain the observed heteroresistance by comparing between the clusters in the pre-treatment bacterial strains. Strains from cluster 2 had a nonsense mutation in *rcsC,* which codes for a histidine kinase of the regulator of capsule synthesis (rcs) system. This system is activated upon cell surface stress, including outer membrane damage, lipopolysaccharide (LPS) synthesis defects, peptidoglycan perturbation and lipoprotein mislocalisation [43]. It subsequently acts as a transcription regulator of associated genes, but also of those related to biofilm formation, motility and virulence [44]. The system regulates the balance between innate and adaptive defence against phages [45-47], and mutations affecting it can confer partial phage-resistance [48]. Cluster 2 also presented missense mutations in genes involved in DNA replication (thymidylate kinase [*tmk*]), amino acid metabolism (shikimate kinase [*aroK*]; 2-aminoadipate transaminase [*lysN*]), and the outer membrane porin *ompP*, although their contribution to decreased susceptibility to øSimón is uncertain.

Finally, we looked for mutations in the post-treatment, phage-selected isolates and found that compared to the wt *B. bronchialis* strain, there was a median of 27 SNPs per strain (range 4 – 32), with no correlation between the number of SNPs and susceptibility to øSimón (Fig. S3 and Supplementary data

364 file). Notably, a bacterial isolate recovered from sputum after 2 days of phage therapy had a total
365 deletion of *btuB,* the gene for the vitamin B12 receptor that we showed was important for øSimón-
366 resistance *in vitro*. This isolate was completely resistant to øSimón. Another isolate from day 2 had a
367 missense mutation in the toxin gene *hipA,* which is part of a known toxin-antitoxin phage defence
368 system [49]. Additionally, we found that many of the phage-selected strains, regardless of their genetic
369 background (cluster 1 or 2), also harboured mutations in cell envelope-associated genes, including cell
370 wall synthesis (*anmK, mrcA, amgK, murB, murU*), LPS biosynthesis (*pgaB, ppgK, waaQ, wecE, gmhB*),
371 LPS export (*lptD, lptG*), and capsular and extracellular polysaccharide synthesis (*wzb*) (Fig. 6f, Table
372 S3), all potentially impacting their susceptibility to øSimón to varying degrees and through different
373 pathways [50-54]. Taken together, these data show that our patient was infected with genetic variants of
374 *B. bronchialis* that had a diverse spectrum of susceptibility to øSimón, even before phage treatment
375 started. After treatment initiation, strains with reduced susceptibility to øSimón persisted, with several
376 defined mutations, including loss of the receptor *btuB,* likely explaining the phenotype. This pre-
377 treatment phage heteroresistance was likely at least partially responsible for the failure of phage therapy
378 in our patient and highlights the potential importance of testing for heteroresistance prior to phage
379 treatment for future patients.

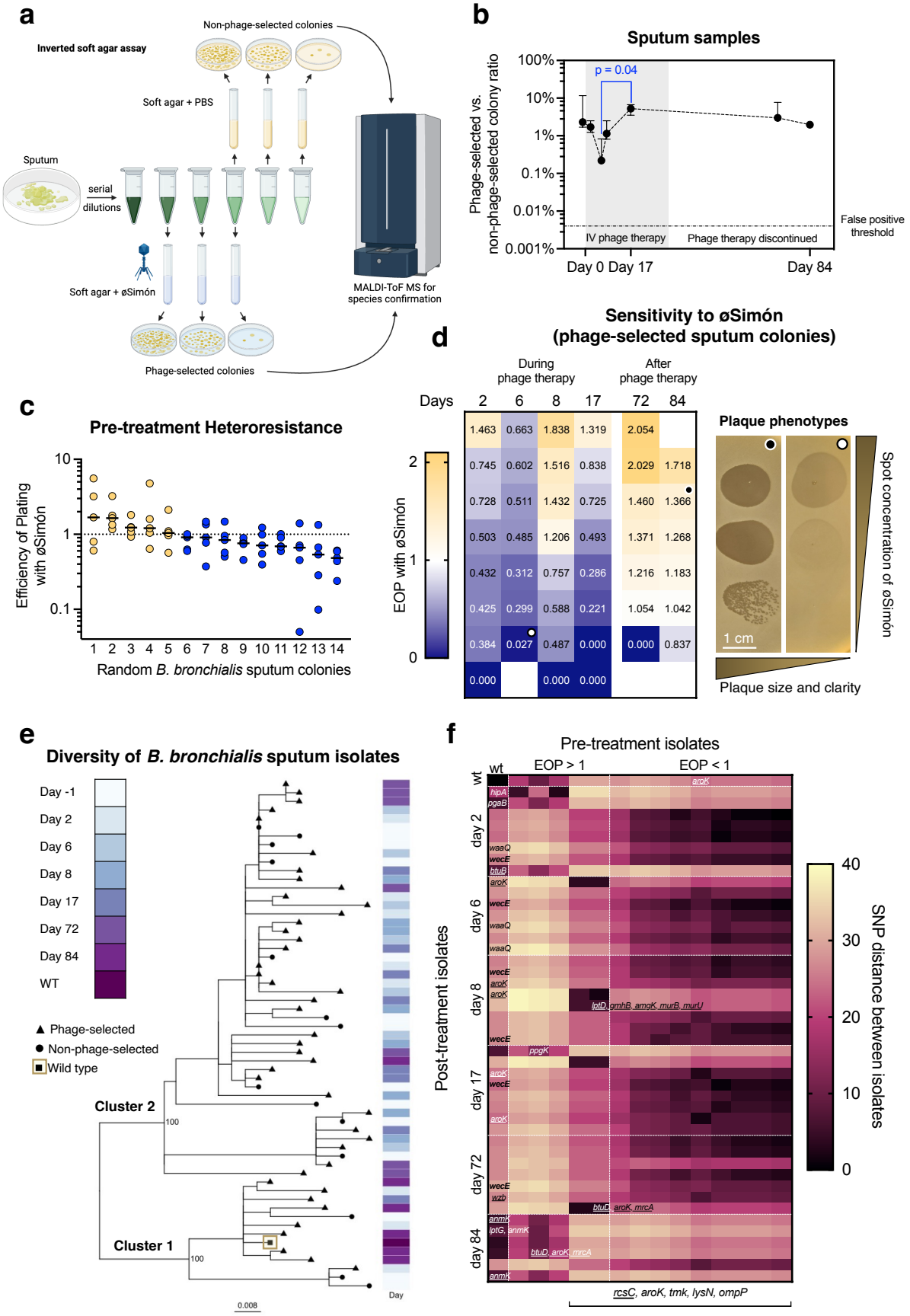
a
Inverted soft agar assay
Non-phage-selected colonies
Soft agar + PBS
Sputum
serial dilutions
Soft agar + øSimón
Phage-selected colonies
MALDI-ToF MS for species confirmation
b
Sputum samples
Phage-selected vs. non-phage-selected colony ratio
100%
10%
1%
0.1%
0.01%
0.001%
p = 0.04
IV phage therapy
Phage therapy discontinued
False positive threshold
Day 0 Day 17
Day 84
c
Pre-treatment Heteroresistance
Efficiency of Plating with øSimón
10
1
0.1
1 2 3 4 5 6 7 8 9 10 11 12 13 14
Random B. bronchialis sputum colonies
d
Sensitivity to øSimón (phage-selected sputum colonies)
During phage therapy
After phage therapy
Days 2 6 8 17 72 84
1.463 0.663 1.838 1.319 2.054
0.745 0.602 1.516 0.838 2.029 1.718
0.728 0.511 1.432 0.725 1.460 1.366
0.503 0.485 1.206 0.493 1.371 1.268
0.432 0.312 0.757 0.286 1.216 1.183
0.425 0.299 0.588 0.221 1.054 1.042
0.384 0.027 0.487 0.000 0.000 0.837
0.000 0.000 0.000
EOP with øSimón
2
1
0
Plaque phenotypes
1 cm
Spot concentration of øSimón
Plaque size and clarity
e
Diversity of B. bronchialis sputum isolates
Day -1
Day 2
Day 6
Day 8
Day 17
Day 72
Day 84
WT
Phage-selected
Non-phage-selected
Wild type
Cluster 2
Cluster 1
100
100
0.008
Day
f
Pre-treatment isolates
wt
EOP > 1
EOP < 1
Post-treatment isolates
day 2
day 6
day 8
day 17
day 72
day 84
hipA
pgaB
waaQ
wecE
btuB
aroK
ppgK
lptD, gmhB, amgK, murB, murU
wzb
btuD, aroK, mrcA
lptG, anmK
rcsC, aroK, tmk, lysN, ompP
SNP distance between isolates
40
30
20
10
0

380

Figure 6. The patient was infected with a heteroresistant bacterial population. a: Phage-selection experiment. Serial dilutions of sputum were mixed with soft agar and either PBS (top) or øSimón (bottom), poured over hard agar plates and incubated. *B. bronchialis* colonies were identified through morphology and MALDI-ToF MS and counted. **b:** The ratio between non-phage-selected (PBS, top in panel a) and phage-selected (øSimón, bottom in panel a) was calculated for each sputum sample timepoint. Dotted line represents the median false positive threshold for the assay calculated on a clonal wt *B. bronchialis* culture (n = 3). Values are median ± 95% CI; n = 3; Kruskal-Wallis test, only p values < 0.05 plotted. **c:** Efficiency of plating (EOP) of øSimón on 14 random colonies from the pre-treatment sputum sample. All replicates plotted; bars are medians. EOPs > 1 in yellow, EOPs < 1 in blue. **d:** Heat map of the sensitivity/resistance spectrum to øSimón of sputum *B. bronchialis*. EOPs (n = 3; median plotted) of 44 phage-selected colonies from 6 different days during and after phage therapy. On the right, representative extremes of plaque size and clarity of øSimón on these strains. The white and black dots at the top right corner of each picture correspond to the strains used in the assay (marked with the same dots in the EOP panel). Scale bar = 1 cm. **e:** Maximum-likelihood tree of the 59 *B. bronchialis* colonies that were sequenced for this study. The tree depicts two clear clusters (100% node support values). **f:** SNP distance matrix between pre-treatment (columns), post-treatment (rows) and wt *B. bronchialis* (upper left corner). Columns ordered left-to-right in descending order of mean SNP distance to post-treatment isolates. Rows ordered by day of treatment and, within days, by descending EOP. The additional vertical dashed line in white separates pre-treatment isolates with EOPs higher and lower than 1, labelled respectively. Gene names in each cell represent mutations in a specific isolate from the rows, discovered after comparison against the corresponding isolate from the columns. The five genes under the heat map are mutated in all isolates of cluster 2, intact in cluster 1. Underlined genes: nonsense mutations or complete deletions; genes in bold: gain-of-function mutations; all the rest: missense mutations. All mutations are further detailed in Table S3 and the Supplementary Data File.

Clinical implications

The resurgence of phage therapy in the context of challenging AMR bacterial infections has highlighted its many remaining unknowns. Here, we provide a detailed analysis of a clinical case of phage therapeutic failure and uncovered important insights with clinical implications for the future care of phage therapy patients. Using longitudinal clinical samples, we first identified the complex dynamics that are taking place between phages, bacteria and human immune responses. When administered intravenously, phage was able to penetrate into the patient's sputum, however phage activity was short-lived. Two main factors appeared to be at play: pre-existing antiphage immunity and bacterial heteroresistance to phage. Importantly, we have shown that in the setting of a chronic bacterial infection, bacterial prophages can act as host immune stimulators, leading to pre-treatment cross-reactive antibodies that can target the therapeutic phage. This pre-treatment phage neutralisation capacity, combined with subpopulations of infecting bacteria with reduced susceptibility to the phage, create a recipe for clinical failure that has been under-appreciated.

We recommend screening a patient's serum for antiphage immunity (serum neutralisation) well before undertaking clinical production of a specific phage. The current Phage Australia clinical protocol suggests testing for antiphage antibodies during and after phage therapy [11]. We suggest that, in the presence of alternative phages suitable for therapy, those that are susceptible to pre-existing immunity should be considered lower priority. Second, we recommend choosing a phage or combination of

423 phages for clinical use by testing them against a patient's bacterial population instead of a single colony.
424 The inverted top agar assay described in this study could be used for that purpose in a cost-effective
425 manner. An increasing amount of evidence recognises that, especially in chronic infections, patients
426 can harbour heterogenous populations of a pathogen [55-57], and a single colony might not be
427 representative of the population's susceptibility to phage therapy. These clinical recommendations are
428 easily applicable to all prospective phage therapy patients but are particularly relevant in patients with
429 recurrent or chronic infections. We hope that as global efforts to bring phage therapy into widespread
430 clinical practice continue, careful analysis of clinical cases and results from well-designed clinical trials
431 will keep providing useful and actionable insights to maximise the effectiveness of this promising
432 antimicrobial strategy.
433

434 **Materials and Methods**

435 **Bacterial growth, quantification, and storage.** *B. bronchialis* was grown on heart infusion (HI) broth
436 (Oxoid, CM1032), supplemented with 1.5% agar, when necessary, aerobically, with constant shaking
437 for liquid cultures, at 37°C for 48 h. Bacterial quantification was performed using the spread-plating
438 technique, with at least two successive 10-fold serial dilutions of the relevant sample yielding countable
439 colonies. When needed, bacterial cultures were diluted 2:3 in 80% glycerol for storage at -80°C.
440

441 **Phage isolation, purification, quantification and efficiency of plating (EOP).** Phage øSimón was
442 isolated from raw sewage samples (Melbourne, VIC, Australia, May 2022). Aliquots of 100 ml of
443 centrifugated and filtered sewage were combined with 1 ml of a turbid *B. bronchialis* liquid culture and
444 supplemented with 10× HI, and 10 mM each of $CaCl_2$ and $MgSO_4$. Mixtures were incubated as above,
445 the resulting lysates were purified with the Phage-on-Tap protocol [58], with or without buffer replacement,
446 for general lab stocks. Phage suspensions needed for Immunology work underwent further purification
447 as performed in [59]. All phage products were stored at 4 °C. Phage quantification and EOP testing were
448 performed with a slightly modified double overlay agar assay [60] using 4 ml of molten soft (0.4%) HI agar
449 and 1 ml of a *B. bronchialis* culture at an optical density (OD_{600}) of 0.3 (previously tested to correspond
450 to a bacterial density of 8×10^8 cfu/ml), per plate. Plates were always read after 48 h of incubation, and
451 the average number of plaques in at least two plates was recorded and compared as a percentage of
452 the plaques formed on the original host of isolation under the same conditions.
453

454 **Bacterial kinetics.** Growth kinetics were determined using a 96-well plate format and
455 spectrophotometry (BioTek Epoch 2), measuring OD_{600} every 15 min with a starting inoculum of 10^6
456 cfu/well, and phage pfu at multiplicities of infection (MOI) of either 0, 0.01, 0.1, or 1.
457

458 **Phage one-step kill curve and adsorption assay.** Bacteria from liquid cultures and phage from a
459 purified stock were mixed at an MOI of 0.01 (10^8 cfu/ml) in HI broth, with cation supplementation as
460 above. The assay was run in 10 ml total volumes. The suspensions were incubated, and at each
461 timepoint, 1 ml samples were taken and filtered with a 0.2 μm syringe filter (Pall, 4612). This filtrate was

462 serially diluted in PBS and plated in duplicate for quantification of free phage particles. A control with no
463 bacteria was routinely run in adsorption assays.
464
465 **Transmission electron microscopy (TEM).** Droplets of phage suspension (10 μl) were placed on
466 copper TEM grids (200 mesh; SPI) with carbon-coated ultrathin formvar film. They were left for 30 s
467 and then dried using filter paper. For negative staining, the grids (face side down) were put to droplets
468 (10 μl) of uranyl acetate water solution (1% w/v) and incubated for 30 s. Finally, the grids were dried
469 with filter paper and examined under a transmission electron microscope (JEM-1400 Plus) at an
470 accelerating voltage of 80 kV. In the induced prophage suspension, imaging was hindered by
471 contamination and low virion concentration.
472
473 **Phage DNA extraction, sequencing and bioinformatics.** One ml volumes of high-titre phage lysate
474 (> 10^8 pfu/ml whenever possible) were treated with DNase (1 mg/ml) and RNase A (12.5 mg/ml) for 2 h
475 at 37 °C, followed by an inactivation step of 5 min at 75 °C. We then used the Norgen phage DNA kit
476 (Norgen Biotek Corp., Thorold, ON, Canada) to extract DNA following the manufacturer's instructions.
477 DNA concentration was measured using a Qubit® Fluorometer, quality confirmed with the 260/280 nm
478 absorbance ratio, and absence of bacterial contamination was confirmed by 16S rRNA PCR and gel
479 visualisation of the DNA samples. Phage øSimón was sequenced on an Illumina HiSeq platform, and
480 with Oxford Nanopore Technologies (ONT) long-read sequencing with a GridION device on FLO-
481 MIN114 R10.4.1 flow cells. The reads were trimmed using trimmomatic (v0.39) [61], assembled with
482 Unicycler (v0.5.0) [62], and annotated using Prokka (v.1.14.6), the RAST server and the PHROG database
483 [63-65]. The genome was set to start at the large terminase subunit (*terL*) gene [66], polished with Pilon
484 (v.1.22) [67]. manually screened for lysogeny indicators and assessed for AMR determinants using
485 AMRFinderPlus (v.3.11.26) [68] and Abricate (v.1.0.1) (https://github.com/tseemann/abricate). Phylogeny
486 was investigated using vContact2 [69] and the gene voting approach [70], both using the Inphared database
487 (version 1Dec2021) [71]. Gene similarity between øSimón and *B. bronchialis* prophages was studied
488 using blastp (v.2.15.0+) and genome maps were visualised using the R package *ggenomes* (v.1.0.0).
489
490 **Production of clinical-grade phage øSimón.** We followed a slightly modified version of a previously
491 used protocol [72]. The phage was amplified in 1,000 ml HI broth. The lysate was centrifugated for 30 min
492 at 4,000 × g to remove larger bacterial debris and then filtered through a depth filter from 5 μm to 0.2
493 μm, monitoring the pressure not to exceed and compromise the filter specifications (<2 bar). The lysate
494 was passed once again through a sterilisation-grade (0.2 μm) filter and transferred to a bacteria-free
495 production facility. The lysate was diluted 1:10 in PBS and flushed through an ÄKTA Flux tangential flow
496 filtration (TFF) system (Cytiva) equipped with a 300 kDa microfiltration hollow fibre cartridge. This
497 process was repeated until the HI broth was completely replaced by PBS. The lysate was filter-sterilised
498 again, and the phage titre measured. Endotoxin removal was performed using EndoTrap®HD affinity
499 columns, and the endotoxin concentration was assessed with Endosafe® PTS™ cartridge (Charles
500 River laboratories, MA, USA) kits. After achieving a satisfactory endotoxin level, we processed the
501 samples under strict sterile conditions, packed them in sealed glass vials with syringe access (Medisca,

502 9497-01), and sent them to Eurofins BioPharma Product Testing in Sydney, Australia for third-party
503 validation for sterility (USP71) and endotoxin (USP85).
504
505 **Handling and storage of clinical specimens.** Serum samples were aliquoted into 200 μl volumes and
506 kept at -20 °C, minimising freeze/thaw cycles. For sputum samples, we first measured their volume and
507 mixed them 1:1 with a 1:10 solution of dithiothreitol (Sputolysin®, CAS 578517) in sterile water with
508 vortexing for 1 min. Bacterial and phage quantification were performed at this stage. For long-term
509 storage for other experiments, each sample was mixed 1:1 with sterile glycerol broth (60 ml glycerol, 2
510 g tryptone, 1 g yeast extract, 2 g NaCl, in 200 ml deionised water) in cryovials and stored at -80 °C.
511
512 **Serum and sputum neutralisation assays and calculation of the phage inactivation rate (*k*).** The
513 clinical samples were diluted 1:10 in PBS, filter-sterilised (0.2 μm syringe filter), and then further diluted
514 in PBS in 10-fold serial dilutions. Working volumes of 1 ml of these dilutions, and a PBS-only control,
515 were spiked with 10^6 pfu each of phages øSimón and øFaith (unpublished phage, isolated in our lab
516 against *Pseudomonas aeruginosa* strains from patients with cystic fibrosis). The samples were
517 incubated at 37 °C for 30 min with constant shaking. At the endpoint, phage quantification using the
518 double overlay agar assay was performed for each phage on their respective hosts of isolation.
519 Neutralisation was calculated as the percentage of active phage at the endpoint compared to the initial
520 phage inoculum for each condition. The phage inactivation rate (*k*) was calculated with the formula:

521 $$k = 2.3 \times \frac{D}{T} \times log \frac{P0}{Pt}$$

522 Where D is the reciprocal of the serum or sputum dilution in PBS, T is the time of incubation, and P0
523 and Pt are the phage titres at the beginning and endpoint of the assay, respectively [15,17].
524
525 **Indirect ELISA and cross-reactive ELISA.** We based our protocol in [16] with some modifications.
526 Individual wells of MICROLON™ high binding 96-well plates (Greiner, 655061) were coated with 100 μl
527 of either pure coating buffer (carbonate-bicarbonate with pH = 9.6, Sigma C3041), phage øSimón
528 calculated at 10^5 pfu/well, induced prophage at 10^3 virions/well, or phage vehicle (obtained after filtering
529 phage solutions with a 0.02 μm syringe filter, Whatman 68091002); the latter three diluted in coating
530 buffer. Plates were covered with foil and incubated at 4 °C for 20 h. The wells were emptied, washed 4
531 times with 300 μl of PBS + 0.05% Tween 80 (PBST), blocked with 200 μl of 3% skim milk powder in
532 PBS, and the plates incubated as above. The blocking solution was shaken off, and the plates patted
533 dry with paper towels. A further blocking step was performed with 3% bovine serum albumin (BSA) in
534 PBS at 37 °C for 30 min, before washing with PBST. The patient samples (serum or filter-sterilised
535 sputum) were diluted in 3% BSA in PBS, added to the respective wells in volumes of 50 μl, incubated
536 at 37 °C for 1 h, and washed with PBST. Next, volumes of 50 μl of 1:500 goat anti-human IgA + IgG +
537 IgM-AP (alkaline phosphatase)-conjugated antibody (RRID: AB_2337605) were added and the plates
538 again incubated and later washed with PBST. Finally, the p-Nitrophenyl phosphate substrate
539 (Sigmafast™, N2770) was added in a volume of 50 μl and the reaction left to develop for 20 min. The
540 assay was stopped by adding 50 μl of 2 M NaOH and the plates were read with a spectrophotometer

541 at 450 nm. For the antibody cross-reactivity testing the same protocol was followed except for a "pre-
542 capture" step involving the passage of individual serum samples by wells covered with øSimón,
543 prophage, or PBS in coating buffer, for 1 h before transferring them into new plates and wells for a
544 regular ELISA as previously described.
545
546 **Prophage induction.** A stationary phase *B. bronchialis* culture was diluted 1:10 in HI and left for
547 incubation for 6 h. The culture was split into two 10 ml aliquots, the first one received a PBS spike
548 (spontaneous induction control), and the second one a mitomycin C at 0.3 mg/ml spike, in equal
549 volumes. Both cultures were left for overnight incubation and purified as above [59]. Prophage induction
550 was confirmed through TEM and phage DNA sequencing.
551
552 **Inverted soft agar assay for phage-selection.** Sputum samples were 10-fold serially diluted in PBS.
553 Then, 100 μl of the dilutions were mixed with 4 ml of molten soft (0.4%) HI agar and 100 μl of either
554 PBS (no phage selection) or a stock of øSimón for a concentration of 10^7 pfu/plate (phage selection),
555 before being poured over plates containing a first layer of standard HI agar. Plates were left for 48 h of
556 incubation and, for counting, *B. bronchialis* colonies on each plate were identified through visual
557 assessment of their morphology, followed by species confirmation using MALDI-ToF MS (Bruker,
558 Biotyper microflex®). Normal microbiota from the upper respiratory tract was consistently seen at
559 concentrations 2 log lower than *B. bronchialis* and thus did not represent a significant confounder in this
560 process. Phage-selected and non-phage-selected colonies underwent two rounds of single-colony
561 purification before being grown in liquid culture and stored as above.
562
563 **Bacterial DNA extraction and sequencing.** Genomic DNA was extracted from *B. bronchialis* cultures
564 using the GenFind V3 Reagent Kit (Beckman Coulter) as per manufacturer's instructions. Illumina
565 libraries were prepared using the Illumina DNA Library Prep Kit, (M) Tagmentaton (Illumina) and
566 sequenced on the Illumina NovaSeq 6000 platform to produce paired-end reads. The wt *B. bronchialis*
567 isolate also underwent long-read Nanopore sequencing with a GridION device on FLO-MIN114 R10.4.1
568 flow cells (Oxford Nanopore Technologies). Sequencing libraries were barcoded with the native
569 barcoding kit SQK-RBK114.96 in accordance with the protocol RBK_9176_v114_revM_27Nov2022.
570
571 **Bacterial genomics.** A *de novo* assembly of the genome of wt *B. bronchialis* was first constructed
572 using Trycycler (v0.5.4) with long read data [73], polished with matching short reads using Polypolish
573 (v0.5.0) [74] and annotated with Bakta (v1.7) [75]. The short-read data from the other isolates also
574 underwent quality control (https://github.com/s-andrews/FastQC) before the genomes were assembled
575 with Unicycler (v0.5.0) [62] and annotated with Prokka (v.1.14.6) [63]. We identified SNPs between the wt
576 *B. bronchialis* reference genome and other sputum isolates using the Nextflow implementation of the
577 Reddog pipeline v1beta.11 using default parameters (https://github.com/scwatts/reddog-nf). The
578 resulting SNP alignment consisted of 250 sites. Complementarily, the wt genome was manually parsed
579 for insertion sequences, whose nucleotide sequences were then mapped against the short reads from
580 other isolates using ISMapper v2.0.0 [76], to detect alternative gene disruptions in these isolates. To

identify the absence of whole genes in pairwise comparisons between isolates we used panaroo (v1.2.4) [77] using thresholds of ≥95% for gene coverage and ≥5x for depth. Phylogeny was studied by constructing a maximum-likelihood tree from the SNP alignment obtained above, with the GTR+Γ model, using RAxML (v8.2.9) [78] with 1,000 bootstrap replicates, then visualised with "ape" (v5.7.1) [79] and "ggtree" (v3.6.2) [80] in R. The pairwise SNP distance matrix was created using "harrietr" (https://github.com/andersgs/harrietr).

Graphing, statistics, and reproducibility. Graphing and statistical analyses were performed with GraphPad Prism 9 (GraphPad Software, Inc.). Figures 4d and 6a were crafted using BioRender. All *in vitro* experiments were performed in triplicate, with at least two technical replicates each. Where appropriate, due to the small number of replicates, medians were presented. To decide between the use of parametric or nonparametric statistical analyses, the data were tested for normality using the Shapiro-Wilk method. The threshold value of two-tailed $p < 0.05$ was used for statistical significance. Observational results, including those from TEM, and phage plaque morphology are representative of at least 100 observations each.

Data availability. All bacterial and phage genomes, sequencing data, and metadata derived from this study have been deposited on NCBI under the BioProject number PRJNA1180749 (Table S4).

Ethical statement. All procedures performed in this study were in accordance with the ethical standards of the institutional research committee (Alfred Hospital Ethics Committee approval number 230/24) and with the Helsinki Declaration (as revised in 2013). Written informed consent to receive phage therapy was obtained from the patient. Data from this clinical case forms part of the STAMP Study [11], trial registration number (registered on ANZCTR 10 Nov 2021): ACTRN12621001526864; WHO Universal Trial Number: U1111-1269-6000.

Acknowledgements

We thank Dr Ryan Burrows (University of Melbourne & Melbourne Water) for his help establishing the collaboration that granted us access to the raw sewage samples used to isolate øSimón. Thanks to Christina Rootes, Dr Christopher Pace, and Dr Duen Siauw for useful feedback on the structure and readability of the manuscript. Thanks to Simón Usúcar Gordillo, after whom phage øSimón was named (que tu vida esté llena de éxito y alegría, tu tío te ama). The Monash Antibody Discovery Platform is supported by funding from Bioplatforms Australia (enabled by NCRIS). This work was supported by Monash eResearch capabilities, including M3, and the Alfred Hospital and Monash University funding of the Victorian Bacteriophage Therapy Program (VICPhage) and the Monash Phage Foundry. Jeremy J. Barr and Anton Y. Peleg also acknowledge the Australian National Health and Medical Research Council (NHMRC) Investigator L1 Grant (2023/GNT2026130) and Practitioner Fellowship (APP1117940), respectively, and the Frontier Health Medical Research support (RFRHPI000017).

621 **Author contributions**

622 Conceptualisation: FGA, JJB, AYP.

623 Laboratory experimental work: FGA, DS, MBu, DMP, MP, DKo, KP, JW, HR.

624 Genomics and bioinformatics: DS, MBe, MBu, SD, JH.

625 Clinical monitoring and follow up: FGA, SK, BJG, YH, DKe, TK, AYP.

626 Data curation, analysis and visualisation: FGA, AYP.

627 Provision of resources: CR, JJB, AYP.

628 Original preparation of the manuscript: FGA, AYP.

629 All authors reviewed, edited and approved the manuscript.

630

631 **Competing interests**

632 None to declare.

633

634 **References**

635 1. G.B.D. Antimicrobial Resistance Collaborators. Global burden of bacterial antimicrobial resistance 1990-
636 2021: a systematic analysis with forecasts to 2050. *Lancet* **404**, 1199-1226 (2024).

637 2. Dadgostar, P. Antimicrobial resistance: implications and costs. *Infect Drug Resist* **12**, 3903-3910 (2019).

638 3. Gordillo Altamirano, F.L. & Barr, J.J. Phage therapy in the postantibiotic era. *Clin Microbiol Rev* **32**(2019).

639 4. Gomez-Ochoa, S.A*., et al.* Efficacy of phage therapy in preclinical models of bacterial infection: a
640 systematic review and meta-analysis. *Lancet Microbe* **3**, e956-e968 (2022).

641 5. Uyttebroek, S*., et al.* Safety and efficacy of phage therapy in difficult-to-treat infections: a systematic review.
642 *Lancet Infect Dis* **22**, e208-e220 (2022).

643 6. Marchi, J., Zborowsky, S., Debarbieux, L. & Weitz, J.S. The dynamic interplay of bacteriophage, bacteria
644 and the mammalian host during phage therapy. *iScience* **26**, 106004 (2023).

645 7. Vandamme, P.A*., et al. Bordetella bronchialis* sp. nov., *Bordetella flabilis* sp. nov. and *Bordetella sputigena*
646 sp. nov., isolated from human respiratory specimens, and reclassification of *Achromobacter sediminum*
647 Zhang *et al.* 2014 as *Verticia sediminum* gen. nov., comb. nov. *Int J Syst Evol Microbiol* **65**, 3674-3682
648 (2015).

649 8. Spilker, T., Darrah, R. & LiPuma, J.J. Complete genome sequences of *Bordetella flabilis, Bordetella*
650 *bronchialis*, and "*Bordetella pseudohinzii*". *Genome Announc* **4**(2016).

651 9. Bridel, S*., et al.* A comprehensive resource for *Bordetella* genomic epidemiology and biodiversity studies.
652 *Nat Commun* **13**, 3807 (2022).

653 10. Suh, G.A*., et al.* Considerations for the use of phage therapy in clinical practice. *Antimicrob Agents*
654 *Chemother* **66**, e0207121 (2022).

655 11. Khatami, A*., et al.* Standardised treatment and monitoring protocol to assess safety and tolerability of
656 bacteriophage therapy for adult and paediatric patients (STAMP study): protocol for an open-label, single-
657 arm trial. *BMJ Open* **12**, e065401 (2022).

658 12. Gembara, K. & Dabrowska, K. Phage-specific antibodies. *Curr Opin Biotechnol* **68**, 186-192 (2021).

659 13. Jerne, N.K. & Avegno, P. The development of the phage-inactivating properties of serum during the course
660 of specific immunization of an animal: reversible and irreversible inactivation. *J Immunol* **76**, 200-208
661 (1956).

662 14. Lusiak-Szelachowska, M., Miedzybrodzki, R., Fortuna, W., Borysowski, J. & Gorski, A. Anti-phage serum
663 antibody responses and the outcome of phage therapy. *Folia Microbiol (Praha)* **66**, 127-131 (2021).

15. Lusiak-Szelachowska, M.*, et al.* Phage neutralization by sera of patients receiving phage therapy. *Viral Immunol* **27**, 295-304 (2014).
16. Dedrick, R.M.*, et al.* Phage therapy of *Mycobacterium* infections: compassionate use of phages in 20 patients with drug-resistant mycobacterial disease. *Clin Infect Dis* **76**, 103-112 (2023).
17. Lusiak-Szelachowska, M.*, et al.* Antiphage activity of sera during phage therapy in relation to its outcome. *Future Microbiol* **12**, 109-117 (2017).
18. Van Belleghem, J.D., Dabrowska, K., Vaneechoutte, M., Barr, J.J. & Bollyky, P.L. Interactions between bacteriophage, bacteria, and the mammalian immune system. *Viruses* **11**(2018).
19. Popescu, M., Van Belleghem, J.D., Khosravi, A. & Bollyky, P.L. Bacteriophages and the immune system. *Annu Rev Virol* **8**, 415-435 (2021).
20. Doria-Rose, N.A. & Joyce, M.G. Strategies to guide the antibody affinity maturation process. *Curr Opin Virol* **11**, 137-147 (2015).
21. Dion, M.B., Oechslin, F. & Moineau, S. Phage diversity, genomics and phylogeny. *Nat Rev Microbiol* **18**, 125-138 (2020).
22. Haddock, N.L., Barkal, L.J. & Bollyky, P.L. Bacteriophage populations mirror those of bacterial pathogens at sites of infection. *mSystems* **8**, e0049723 (2023).
23. Haddock, N.L.*, et al.* Phage diversity in cell-free DNA identifies bacterial pathogens in human sepsis cases. *Nat Microbiol* **8**, 1495-1507 (2023).
24. Nayfach, S.*, et al.* CheckV assesses the quality and completeness of metagenome-assembled viral genomes. *Nat Biotechnol* **39**, 578-585 (2021).
25. Halperin, S.A., Ferrieri, P., Gray, E.D., Kaplan, E.L. & Wannamaker, L.W. Antibody response to bacteriophage hyaluronidase in acute glomerulonephritis after group A streptococcal infection. *J Infect Dis* **155**, 253-261 (1987).
26. Fluckiger, A.*, et al.* Cross-reactivity between tumor MHC class I-restricted antigens and an enterococcal bacteriophage. *Science* **369**, 936-942 (2020).
27. Berkson, J.D.*, et al.* Phage-specific immunity impairs efficacy of bacteriophage targeting Vancomycin Resistant *Enterococcus* in a murine model. *Nat Commun* **15**, 2993 (2024).
28. Egido, J.E., Costa, A.R., Aparicio-Maldonado, C., Haas, P.J. & Brouns, S.J.J. Mechanisms and clinical importance of bacteriophage resistance. *FEMS Microbiol Rev* **46**(2022).
29. Labrie, S.J., Samson, J.E. & Moineau, S. Bacteriophage resistance mechanisms. *Nat Rev Microbiol* **8**, 317-327 (2010).
30. Lebeaux, D.*, et al.* A case of phage therapy against pandrug-resistant *Achromobacter xylosoxidans* in a 12-year-old lung-transplanted cystic fibrosis patient. *Viruses* **13**(2021).
31. Blasco, L.*, et al.* Case report: analysis of phage therapy failure in a patient with a *Pseudomonas aeruginosa* prosthetic vascular graft infection. *Front Med (Lausanne)* **10**, 1199657 (2023).
32. Jault, P.*, et al.* Efficacy and tolerability of a cocktail of bacteriophages to treat burn wounds infected by *Pseudomonas aeruginosa* (PhagoBurn): a randomised, controlled, double-blind phase 1/2 trial. *Lancet Infect Dis* **19**, 35-45 (2019).
33. Schooley, R.T.*, et al.* Development and use of personalized bacteriophage-based therapeutic cocktails to treat a patient with a disseminated resistant *Acinetobacter baumannii* infection. *Antimicrob Agents Chemother* **61**(2017).
34. Gordillo Altamirano, F.L.*, et al.* Phage-antibiotic combination is a superior treatment against *Acinetobacter baumannii* in a preclinical study. *EBioMedicine* **80**, 104045 (2022).
35. Zhvania, P., Hoyle, N.S., Nadareishvili, L., Nizharadze, D. & Kutateladze, M. Phage therapy in a 16-year-old boy with Netherton syndrome. *Front Med (Lausanne)* **4**, 94 (2017).

36. Bertozzi Silva, J., Storms, Z. & Sauvageau, D. Host receptors for bacteriophage adsorption. *FEMS Microbiol Lett* **363**(2016).
37. Happonen, L.J., Pajunen, M.I., Jun, J.W. & Skurnik, M. BtuB-dependent infection of the T5-like *Yersinia* phage varphiR2-01. *Viruses* **13**(2021).
38. Hong, J.*, et al.* Identification of host receptor and receptor-binding module of a newly sequenced T5-like phage EPS7. *FEMS Microbiol Lett* **289**, 202-209 (2008).
39. Golomidova, A.K.*, et al.* Branched lateral tail fiber organization in T5-like bacteriophages DT57C and DT571/2 is revealed by genetic and functional analysis. *Viruses* **8**(2016).
40. Gordillo Altamirano, F.L. & Barr, J.J. Unlocking the next generation of phage therapy: the key is in the receptors. *Curr Opin Biotechnol* **68**, 115-123 (2021).
41. Gillis, A. & Mahillon, J. An improved method for rapid generation and screening of *Bacillus thuringiensis* phage-resistant mutants. *J Microbiol Methods* **106**, 101-103 (2014).
42. Andersson, D.I., Nicoloff, H. & Hjort, K. Mechanisms and clinical relevance of bacterial heteroresistance. *Nat Rev Microbiol* **17**, 479-496 (2019).
43. Meng, J., Young, G. & Chen, J. The Rcs system in *Enterobacteriaceae*: envelope stress responses and virulence regulation. *Front Microbiol* **12**, 627104 (2021).
44. Wall, E., Majdalani, N. & Gottesman, S. The complex Rcs regulatory cascade. *Annu Rev Microbiol* **72**, 111-139 (2018).
45. Chaudhry, W.*, et al.* Mucoidy, a general mechanism for maintaining lytic phage in populations of bacteria. *FEMS Microbiol Ecol* **96**(2020).
46. Mutalik, V.K.*, et al.* High-throughput mapping of the phage resistance landscape in *E. coli*. *PLoS Biol* **18**, e3000877 (2020).
47. Smith, L.M.*, et al.* The Rcs stress response inversely controls surface and CRISPR-Cas adaptive immunity to discriminate plasmids and phages. *Nat Microbiol* **6**, 162-172 (2021).
48. Burmeister, A.R., Tewatia, H. & Skinner, C. A tradeoff between bacteriophage resistance and bacterial motility is mediated by the Rcs phosphorelay in *Escherichia coli*. *Microbiology (Reading)* **170**(2024).
49. LeRoux, M. & Laub, M.T. Toxin-antitoxin systems as phage defense elements. *Annu Rev Microbiol* **76**, 21-43 (2022).
50. Kortright, K.E., Chan, B.K. & Turner, P.E. High-throughput discovery of phage receptors using transposon insertion sequencing of bacteria. *Proc Natl Acad Sci U S A* **117**, 18670-18679 (2020).
51. Acton, L.*, et al.* Collateral sensitivity increases the efficacy of a rationally designed bacteriophage combination to control *Salmonella enterica*. *J Virol*, e0147623 (2024).
52. Bai, J., Raustad, N., Denoncourt, J., van Opijnen, T. & Geisinger, E. Genome-wide phage susceptibility analysis in *Acinetobacter baumannii* reveals capsule modulation strategies that determine phage infectivity. *PLoS Pathog* **19**, e1010928 (2023).
53. Nyenhuis, D.A., Nilaweera, T.D. & Cafiso, D.S. Native cell environment constrains loop structure in the *Escherichia coli* cobalamin transporter BtuB. *Biophys J* **119**, 1550-1557 (2020).
54. Shearer, J., Jefferies, D. & Khalid, S. Outer membrane proteins OmpA, FhuA, OmpF, EstA, BtuB, and OmpX have unique lipopolysaccharide fingerprints. *J Chem Theory Comput* **15**, 2608-2619 (2019).
55. Dewachter, L., Fauvart, M. & Michiels, J. Bacterial heterogeneity and antibiotic survival: understanding and combatting persistence and heteroresistance. *Mol Cell* **76**, 255-267 (2019).
56. Klein, S.*, et al.* Comparative genomic reveals clonal heterogeneity in persistent *Staphylococcus aureus* infection. *Front Cell Infect Microbiol* **12**, 817841 (2022).
57. Bartell, J.A.*, et al.* Evolutionary highways to persistent bacterial infection. *Nat Commun* **10**, 629 (2019).

753 58. Bonilla, N., *et al.* Phage on tap-a quick and efficient protocol for the preparation of bacteriophage laboratory
754 stocks. *PeerJ* **4**, e2261 (2016).
755 59. Bichet, M.C., Patwa, R. & Barr, J.J. Protocols for studying bacteriophage interactions with in vitro epithelial
756 cell layers. *STAR Protoc* **2**, 100697 (2021).
757 60. Stachurska, X., Roszak, M., Jablonska, J., Mizielinska, M. & Nawrotek, P. Double-layer agar (DLA)
758 modifications for the first step of the phage-antibiotic synergy (PAS) identification. *Antibiotics (Basel)*
759 **10**(2021).
760 61. Bolger, A.M., Lohse, M. & Usadel, B. Trimmomatic: a flexible trimmer for Illumina sequence data.
761 *Bioinformatics* **30**, 2114-2120 (2014).
762 62. Wick, R.R., Judd, L.M., Gorrie, C.L. & Holt, K.E. Unicycler: Resolving bacterial genome assemblies from
763 short and long sequencing reads. *PLoS Comput Biol* **13**, e1005595 (2017).
764 63. Seemann, T. Prokka: rapid prokaryotic genome annotation. *Bioinformatics* **30**, 2068-2069 (2014).
765 64. Aziz, R.K., *et al.* The RAST Server: rapid annotations using subsystems technology. *BMC Genomics* **9**, 75
766 (2008).
767 65. Terzian, P., *et al.* PHROG: families of prokaryotic virus proteins clustered using remote homology. *NAR*
768 *Genom Bioinform* **3**, lqab067 (2021).
769 66. Shen, W., Le, S., Li, Y. & Hu, F. SeqKit: A Cross-Platform and Ultrafast Toolkit for FASTA/Q File
770 Manipulation. *PLoS One* **11**, e0163962 (2016).
771 67. Walker, B.J., *et al.* Pilon: an integrated tool for comprehensive microbial variant detection and genome
772 assembly improvement. *PLoS One* **9**, e112963 (2014).
773 68. Feldgarden, M., *et al.* AMRFinderPlus and the Reference Gene Catalog facilitate examination of the
774 genomic links among antimicrobial resistance, stress response, and virulence. *Sci Rep* **11**, 12728 (2021).
775 69. Bin Jang, H., *et al.* Taxonomic assignment of uncultivated prokaryotic virus genomes is enabled by gene-
776 sharing networks. *Nat Biotechnol* **37**, 632-639 (2019).
777 70. Nayfach, S., *et al.* Metagenomic compendium of 189,680 DNA viruses from the human gut microbiome. *Nat*
778 *Microbiol* **6**, 960-970 (2021).
779 71. Cook, R., *et al.* INfrastructure for a PHAge REference Database: identification of large-scale biases in the
780 current collection of cultured phage genomes. *Phage (New Rochelle)* **2**, 214-223 (2021).
781 72. Subedi, D., *et al.* Rational design of frontline institutional phage cocktail for the treatment of nosocomial
782 *Enterobacter cloacae* complex infections. Preprint at
783 https://www.biorxiv.org/content/10.1101/2024.06.30.601436v2 (2024).
784 73. Wick, R.R., *et al.* Trycycler: consensus long-read assemblies for bacterial genomes. *Genome Biol* **22**, 266
785 (2021).
786 74. Wick, R.R. & Holt, K.E. Polypolish: Short-read polishing of long-read bacterial genome assemblies. *PLoS*
787 *Comput Biol* **18**, e1009802 (2022).
788 75. Schwengers, O., *et al.* Bakta: rapid and standardized annotation of bacterial genomes via alignment-free
789 sequence identification. *Microb Genom* **7**(2021).
790 76. Hawkey, J., *et al.* ISMapper: identifying transposase insertion sites in bacterial genomes from short read
791 sequence data. *BMC Genomics* **16**, 667 (2015).
792 77. Tonkin-Hill, G., *et al.* Producing polished prokaryotic pangenomes with the Panaroo pipeline. *Genome Biol*
793 **21**, 180 (2020).
794 78. Stamatakis, A. RAxML version 8: a tool for phylogenetic analysis and post-analysis of large phylogenies.
795 *Bioinformatics* **30**, 1312-1313 (2014).
796 79. Paradis, E. & Schliep, K. ape 5.0: an environment for modern phylogenetics and evolutionary analyses in R.
797 *Bioinformatics* **35**, 526-528 (2019).

80. Yu, G. Using ggtree to visualize data on tree-like structures. *Curr Protoc Bioinformatics* **69**, e96 (2020).